IEEE Open Access Journal of
Power and Energy

Received 16 May 2023; revised 3 August 2023; accepted 2 September 2023.
Date of publication 7 September 2023; date of current version 22 September 2023.

Digital Object Identifier 10.1109/OAJPE.2023.3312640

Ferroresonance Modeling and Analysis in Underground Distribution Feeders

V. TORRES-GARCÍA[1] (Senior Member, IEEE), N. SOLÍS-RAMOS[2] (Member, IEEE), N. GONZÁLEZ-CABRERA[3] (Member, IEEE), E. HERNÁNDEZ-MAYORAL[4] (Member, IEEE), AND DANIEL GUILLEN[5] (Senior Member, IEEE)

[1]PGIIE, National Technological Institute of Mexico, Morelia City 58120, México
[2]Federal Electricity Commission, Mexico City 06600, México
[3]Faculty of Engineering, National Autonomous University of México (UNAM), México City 04510, México
[4]Institute of Renewable Energies, National Autonomous University of México (UNAM), Temixco 62580, México
[5]School of Engineering and Sciences, Tecnologico de Monterrey, Monterrey, Nuevo León 64890, México
CORRESPONDING AUTHOR: V. TORRES-GARCÍA (v.torres@ieee.org)

ABSTRACT Nowadays, many modern electrical power systems are designed for transmission and distribution using underground systems. Such systems minimize visual impact, reduce congestion, and increase security and reliability. However, the technology utilized has increased the capacitance effect, which can lead to the system being more susceptible to the occurrence of the ferroresonance phenomenon. Ferroresonance can cause dielectric or thermal damage and consequently makes the system susceptible to faults in the electrical power equipment and installations. This paper analyzes the ferroresonance phenomenon after switching maneuvers in a real underground distribution feeder to detect possible conditions of ferroresonance. The analysis is carried out in a typical underground distribution system with distribution transformers connected in wye-grounded/wye-grounded (Ynyn), and modeled using the ATP/EMTP software.

INDEX TERMS Distribution systems, ferroresonance, power cables, power quality, and underground lines.

I. INTRODUCTION

THE use of underground cables has increased in recent years intending to reduce congestion and environmental impact, as well as for the interconnection of new renewable energy systems such as wind and photovoltaic power plants. This technology change for energy transmission through underground cables increases the capacitance effect of the system. In consequence, natural resonance frequencies close to the nominal frequency of the system can give place to unwanted phenomena such as resonance and ferroresonance [1].

The phenomenon of ferroresonance is characterized by the presence of overvoltages (OV) caused by non-linear oscillations due to the interaction between capacitance and non-linear inductance. The non-linear inductance is a property of the iron core of transformers which not only can operate in the saturated region but also resonate with the system capacitance, taking place transient unwanted overvoltages [2]. Such overvoltages can cause dielectric or thermal damage to electrical installations and the power equipment, leading to detrimental effects on system reliability and security.

Over the years, the phenomenon has been analyzed and measured and various techniques, methods, and models have been developed to mitigate the ferroresonance occurrence. However, the mitigation remains under study because it is an unpredictability phenomenon due to the lack of understanding.

Over the last years, a variety of techniques have been proposed to study ferroresonance in three-phase transformers. For instance, in [3] the stochastic behavior of ferroresonance is analyzed, showing that the parameters are fundamental in the phenomenon analysis. In [4] the methodology is developed through mathematical analysis, which is verified by an experimental test; in [5] an analysis of thermal behavior of the transformer under ferroresonance condition is also studied by using a finite element model.

On the other hand, the elimination of ferroresonance is explored in [6] where a switching control by using coefficients of the proportional-integral (PI) controller is utilized to suppress the ferroresonance. In [7] an inductive superconducting fault current limiter is proposed, and more recently in [8] a method to reduce the ferroresonace overvoltage is

proposed by using High Ohmic Reactor (HOR) as a Shunt Limiter (SL). That technique is based on the measurements of the negative sequence components.

Finally, it is known that the ferroresonance condition can be presented in underground distribution systems such as wind energy and solar conversion systems, for example in [9] possible scenarios of ferroresonance in wind farms that can lead to ferroresonance are investigated. In this way, in [10] the ferroresonance associated with a single-pole outage of the line breaker is mitigated by fast regulating the reactive power using the static compensator (STATCOM); in [11] an adaptive algorithm designated to overcurrent relay to distinguish the ferroresonance from other phenomena is presented. Also, in [12] an ungrounded distribution system of a solar power plant shows that high unbalance in medium voltage can lead to ferroresonance.

In this paper, the ferroresonance phenomenon in underground distribution feeders during maneuvers is analyzed to show the conditions that give place to the phenomenon and provide the surge arresters energy behavior and risk of damage. The simulations are carried out representing a real scenario of an underground distribution system of 23 kV with distribution transformers connected in wye/grounded-wye/grounded (Ynyn) by using the ATP/EMTP software [13].

The main contributions of this paper are the assessment and steps to modeling and evaluating the ferroresonance in underground feeders. These are summarized as follows:

- Modeling the single RLC circuit with non-linear inductance by using a polynomial function.
- Modeling of a real distribution feeder in underground systems of 23 kV.
- Assessment and impact of switching time on and off in typical underground feeders.
- Assessment of ferroresonance occurring in a distribution transformer, with YNyn connection.
- Assessment of the surge arrester and dissipated energy during the ferroresonance phenomenon.

II. FERRORESONANCE PHENOMENON AND MODELING

A. FERRORESONANCE

The term ferroresonance is described as a complex resonant oscillation in an RLC circuit with *non-linear* inductance [1]. Furthermore, the phenomenon distorts the voltage signal in the form of non-periodic oscillations that cause transient overvoltages, mainly in circuits with *power transformers*, *voltage transformers (VT's)* and *capacitive voltage transformers (CVT's)*. Ferroresonance can be founded in four modes: fundamental, sub-harmonic, quasi-periodic, and chaotic [14].

This phenomenon must be considered in the design of electrical systems since it draws overvoltages that can cause damage to power equipment and installations. For the study of ferroresonance, several configurations that can produce the phenomenon have been found in the literature [15], as follows:

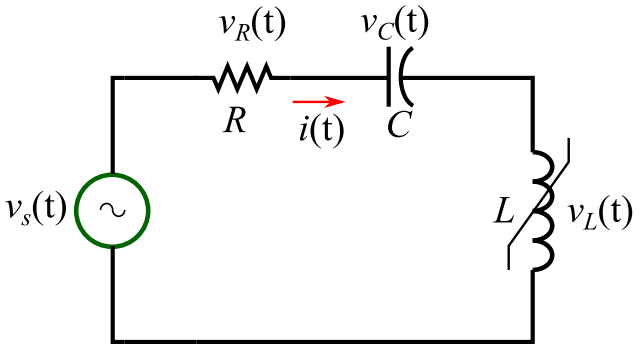

FIGURE 1. **RLC circuit with non-linear inductance.**

- Transformer switching in one or two phases.
- Transformer energized through the capacitive gradient in one or two open circuit breakers.
- Transformer connected into a series with a compensated transmission line.
- Voltage Transformer (VT) connected to an isolated neutral system.
- Capacitor Voltage Transformer (CVT).
- Transformer connected to a de-energized transmission line running in parallel with an energized line.
- Transformer supplied through a long transmission line or cable with low short-circuit power.

B. FERRORESONANCE MODELING

Figure 1 shows a single-phase equivalent circuit for analyzing series ferroresonance, which consists of a series resistance R, capacitance C, and non-linear inductance L. The general equation derived from Kirchhoff's Voltage Law (KVL) is defined by:

$$v_s(t) = Ri(t) + \frac{1}{C}\int i(t)\,dt + L\frac{di(t)}{dt} \tag{1}$$

For a linear RLC circuit, the equation (1) can be solved for $i(t)$ taking into consideration the boundary conditions. In fact, the input represents an AC voltage signal such as:

$$v_s(t) = V_{max}sin(\omega t + \theta) \tag{2}$$

where V_{max} is the peak voltage, ω represents the angular frequency, and θ is the phase angle.

The numerical solution for the expression (1) in the presence of a non-linear inductance is more complex than a numerical solution to a simple RLC circuit. This is because the current is a function of the magnetic flux λ, this entails that the non-linear inductance saturation curve must be modeled as a function of the magnetic flux, and one of the most common expressions to that purpose is by means of a polynomial equation such as [16]:

$$i(\lambda) = a\lambda^3 + b\lambda^2 + c\lambda + d \tag{3}$$

From Figure 1, the loop current based on the magnetic flux will be $i(\lambda) = i_R(\lambda) = i_L(\lambda) = i_C(\lambda)$. Additionally, it is

well-known that

$$v_L(t) = L\frac{di(t)}{dt} \tag{4}$$

$$i_C(t) = C\frac{dv_c(t)}{dt} \tag{5}$$

Therefore, all terms in (1) can be represented in the same domain as follows:

$$v_L(t) = \frac{d\lambda}{dt} \tag{6}$$

$$\frac{dv_C(t)}{dt} = \frac{i_C(\lambda)}{C} = \frac{1}{C}(a\lambda^3 + b\lambda^2 + c\lambda + d) \tag{7}$$

Deriving expression (1) with respect to t and considering (2), we have:

$$\omega V_{max} cos(\omega t + \theta) = R\frac{di(\lambda)}{dt} + \cdots + \frac{1}{C}(a\lambda^3 + b\lambda^2 + c\lambda + d) + \frac{d^2\lambda}{dt^2} \tag{8}$$

where

$$\frac{di(\lambda)}{dt} = \frac{i(\lambda)}{d\lambda}\frac{d\lambda}{dt}$$

$$\frac{di(\lambda)}{dt} = (3a\lambda^2 + 2b\lambda + c)\frac{d\lambda}{dt}$$

Finally, equation (1) can be represented in terms of λ such as:

$$\omega V_{max} cos(\omega t + \theta) = R(3a\lambda^2 + 2b\lambda + c)\frac{d\lambda}{dt} + \cdots + \frac{a\lambda^3 + b\lambda^2 + c\lambda + d}{C} + \frac{d^2\lambda}{dt^2} \tag{9}$$

The above equation (9) is a non-linear second-order differential equation, where the analytical solution is very complex; in this context, a wide variety of methods to solve it have been carried out, for example, the Ritz harmonic balance method was one of the first introduced methods [17], which allowed computing ferroresonant regions in the power system depending on the circuit parameters. On the other hand, the well-known Galerkin method was proposed in [18], and emerged as another alternative to resolve the ferroresonant circuit. Also, the theory of non-linear system dynamics was proposed and discussed in [19]. Currently, other models have been explored such as [20], where a dynamic model of the transformer takes into account the dependence of frequency and peak induction which is implemented with the aim of identifying the stability at critical points and in [21] modeled the core hysteresis loop and the electromagnetic and thermal behaviors are analyzed during ferroresonance.

In spite of the complexity of the non-linear second-order differential equation, its solution can be simultaneously solved with two first-order differential equations from the equations (10) and (11), as shown below:

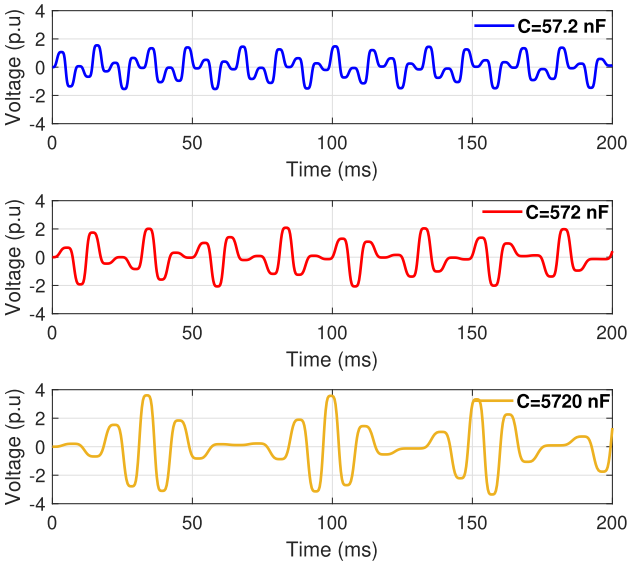

FIGURE 2. **Inductance voltage.**

$$\frac{d\lambda}{dt} = V_{max} sin(\omega t + \theta) - R(a\lambda^3 + b\lambda^2 + c\lambda + d) - v_C(\lambda) \tag{10}$$

$$\frac{dv_C(t)}{dt} = \frac{dv_C(\lambda)}{dt} = \frac{1}{C}(a\lambda^3 + b\lambda^2 + c\lambda + d) \tag{11}$$

Taking into account the equations (10) and (11), one can lead to a practical solution where the capacitance plays a key role in the resonance phenomenon. For example, a typical underground distribution feeder is studied with typical positive sequence parameters such as $Z_1 = 0.0542$+j$0.1826\ \Omega$ and $C_1 = 572\ n$F corresponding to the total length of the cable of 1.45 km, operating at 23 kV. The feeder consists of a distribution transformer whose ratings are 23/0.22 kV, 500 kVA, and 60 Hz, and is represented by its saturation curve. To show the relevance of the capacitive effect, the distribution feeder is modeled by the simplified circuit shown in Figure 1, such that the capacitance varies from 57.2nF up to 5720nF. Following Figure 1, the simulations are carried out to obtain the voltage through the inductor whose results are depicted in Figure 2 dependent on the capacitance used. Figure 2a) shows that a capacitance value of $C_1 = 57.2\ n$F generates an overvoltage equal to 1.47 p.u.; for $C_1 = 572\ n$F the overvoltage is around 2.08 p.u., and with $C_1 = 5720\ n$F, the overvoltage through the inductor reaches 3.56 p.u. Based on the results, it should be mentioned that lower values of capacitance will not show overvoltage, this demonstrates that the overvoltages caused by the ferroresonance phenomenon have a high dependency on the capacitance and non-linear inductance.

In general, the capacitance presents a high sensitivity associated with the ferroresonance in the system that is under study. It should be mentioned that the studied model is represented by a single-phase equivalent and the coupling among

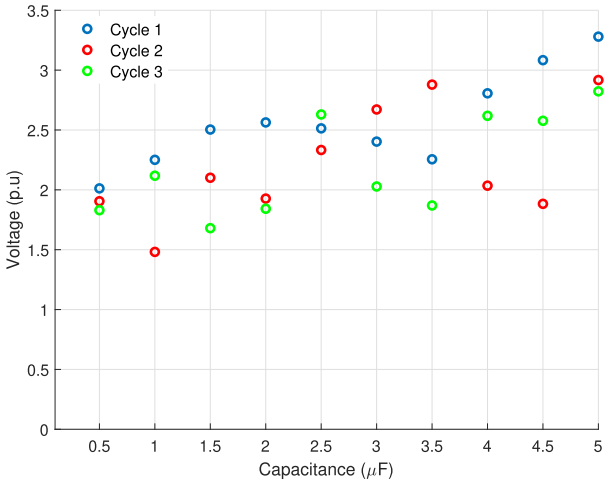

FIGURE 3. Bifurcation diagram.

phases is not considered. On the other hand, the voltage may vary per cycle so the bifurcation diagram may help in understanding the essential dynamics of voltage behavior. In fact, the bifurcation diagram is a collection of many Poincaré sections, each one calculated for a different value of a particular parameter of the system [22]. In this sense, Figure 3 shows the effect of varying the capacitance in the simplified circuit corresponding to Figure 1. From Figure 3, there are different voltage magnitudes during the first cycles for several capacitance values. In this graph, three cycles were evaluated showing the peak voltage magnitude for each cycle considered in the analysis. In addition, in Figure Figure 3, one can observe the range of the voltage magnitudes between 1.5 p.u. and 3.3 p.u., resulting from the capacitance variations.

Despite the complex analytical solution of the ferroresonance phenomena, the analysis can be considerably simplified by limiting the calculations to the steady-state frequency of the system [23]. The non-linear inductance represents the magnetic core saturation of the transformer, therefore, the resonance frequency is variable, so that for a wide variety of capacitances, the electric circuit can lead to ferroresonance, where it hopes harmonic components into the voltage and current waveforms caused by the presence of the nonlinear inductances. In fact, if it is considered that R is small compared with the inductive reactance X_L and the capacitive reactance X_C, equation (1) can be simplified as follows

$$v_s(t) = v_C(t) + v_L(t) \tag{12}$$

Equation (12) can also be expressed in the phasor domain as follows:

$$V_s = V_C + V_L \tag{13}$$

Then, equation (13) will be an expression that is a function of I, where $V_L = jIX_L(I)$, this means that the characteristics of the ferromagnetic inductance depend on parameters such as permeability, the number of turns, and the dimensions of the iron core, such as

$$V_s = -jIX_C + jIX_L(I) \tag{14}$$

where $X_L(I)$ is the variable reactance in the magnetic core, X_C is the capacitive reactance in steady-state, $X_C = \frac{1}{w_s C}$, and w_s represents the angular frequency in steady-state.

The graphical representation of equations (13) and (14) is shown in Figure 4, where it shows, the slope of the straight line that represents V_C, intersecting the curve associated with V_L, giving place to the ferroresonance phenomenon. In addition, it can be highlighted three points of the intersection that can be interpreted as follows:

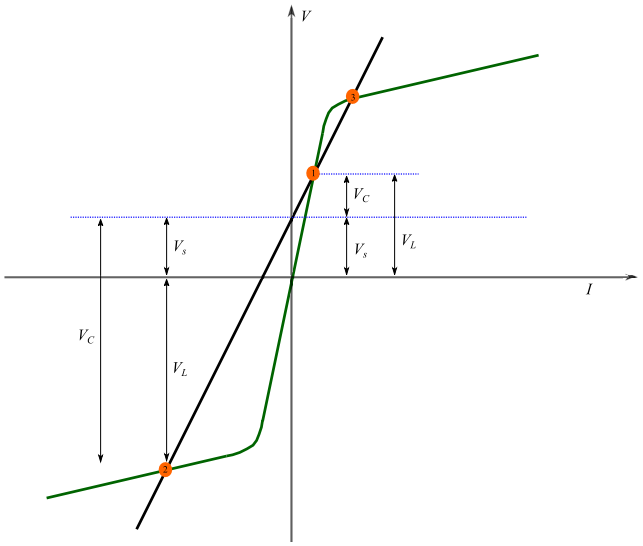

FIGURE 4. Ferroresonance points.

From Figure 4, Point 1 which is the intersection of (13) and (14), is considered a normal operation point, where the circuit is operating in its inductive mode, where V_C corresponds to the voltage of the capacitor and V_L the voltage in the inductor. In the Figure, it can be observed that, if only the source voltage V_s were applied to the capacitor, then there is a large current I_C. In Point 2, the capacitive voltage is greater than the inductive voltage and the source voltage. This is also a stable solution. Finally, if a momentary change occurs in I_L, Point 3, would cause changes in V_L and V_C, and can destabilize the system and represents a solution of the circuit but its behavior is unstable.

III. FERRORESONANCE IN UNDERGROUND DISTRIBUTION FEEDERS

A. UNDERGROUND CABLES

Until recently, the utilization of underground cables in distribution systems has noticeably increased. Such cable systems are often proposed to protect the environment and also public health, which intrinsically improves the reliability of the electrical network and reduces the visual impact.

The most utilized cables in distribution networks are the cross-linked polyethylene (XLPE), and its use began

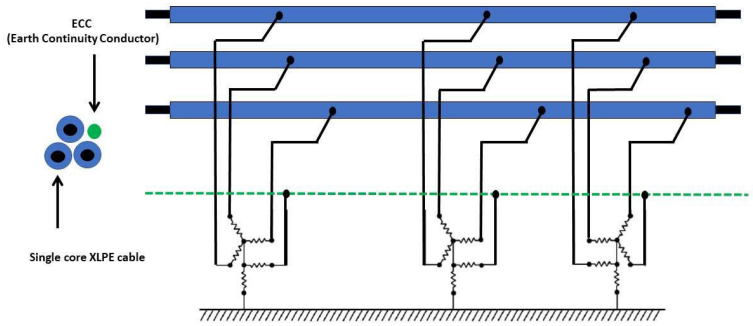

FIGURE 5. **Medium voltage cable system configuration used in the study.**

in 1960 [24]. Some reasons associated with the use of XLPE cables are the minimal maintenance required, no pressure preservation systems required, being harmless to the environment, and good operating experience.

The typical distribution feeder configuration utilized in the underground system is the three coaxial cables and one bare conductor that works as the Earth Continuity Conductor (ECC) as shown in Figure 5. Such cable system is implemented in the ATP/EMTP software as follows:

- The central conductor must be represented in ATP/EMTP with a solid conductor with the data of inner radius $Rin(m)$, outer radius $Rout(m)$, resistivity $\rho(ohm.m)$ at direct current and relative magnetic permeability μ.
- The cable data is provided by the manufacturer and includes the effective cross-section A in mm^2, the resistivity of the material ρ, as well as the inner diameter Din, and the outer diameter De expressed in millimeters (mm).
- In the ATP/EMTP should consider three concentric layers on the central bundle of conductive wires: inner semiconductor, main insulation, and outer semiconductor. This group of layers has the capacitive behavior of the main insulation and must be represented in the ATP/EMTP, with the data of relative permittivity ϵ_r and relative permeability μ_r and its outer radius which is the inner radius $Ri(m)$. The inner radius of the insulation is the outer radius $Rout(m)$.
- Then, the cable data, provided by the manufacturer, include the permittivity relative ϵ_r of the material, as well as the diameters on the cover inner semiconductor Dsi (mm), the main insulation $Da(mm)$ and the outer semiconductor jacket $Dse(mm)$. It is assumed that the relative permeability, $\mu = 1$.
- Finally, a concentric insulation layer must be represented in the ATP/EMTP software with a unique "Sheath" tubular insulation section, and with the relative permittivity $\epsilon(ins)$, the relative permeability $\mu(ins)$ and the total outer radius $Rout(m)$ of the cable.

The cable data employed in this work were obtained directly from the manufacturers [25], and are processed into the ATP/EMTP software for their characterization.

B. DISTRIBUTION TRANSFORMERS

The three-phase distribution transformers commonly used by the electric utility in México for underground service are normally single units, usually on a three-, four-, or five-legged core. The five-legged wound core transformer is very common. Also, there are many types of three-phase connections used to serve three-phase load on distribution systems (ANSI/IEEE C57.105-1978) [26], in which the primary and secondary windings may be connected in different ways, such as delta, wye-grounded or wye-ungrounded in the primary side. The characteristics are:

- Ungrounded primary - The delta and ungrounded-wye primary connections are suitable for ungrounded and grounded distribution systems. Ferroresonance is more likely with ungrounded primary connections (typically utilized in the wind and photovoltaic parks).
- Grounded primary - The grounded-wye primary connection is only suitable on four-wire grounded systems (either multi-grounded or ungrounded), which is not for use on ungrounded systems. The Ferroresonance can be presented with a four or five-legged core construction (typically utilized in the underground distribution grids).

The equivalent circuit of the transformer in ATP/EMTP is shown in Figure 6, which is considered the saturation curve. On the other hand, the saturation in the transformers is an important characteristic that has been taken into account for the ferroresonance phenomenon, mainly when the transformer operates in the saturation zone. There are several methods for obtaining the saturation curve of the non-linear inductive element [27], Figure 7 shows the typical transformer non-linear saturation curve, which is directly related to the nameplate capacity and is reported in Table 1 taking the *RMS* values.

C. SURGE ARRESTER MODEL

For temporary overvoltage, the common protection utilized in electrical equipment such as distribution transformers is the surge arresters. The Sustained overvoltage under ferroresonance conditions could stress the equipment and would cause surge arresters to conduct over extended periods exceeding their energy dissipation capabilities and damaging them. In a

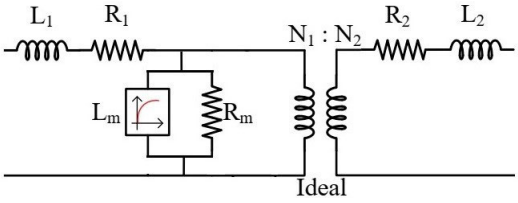

FIGURE 6. Equivalent circuit of transformer.

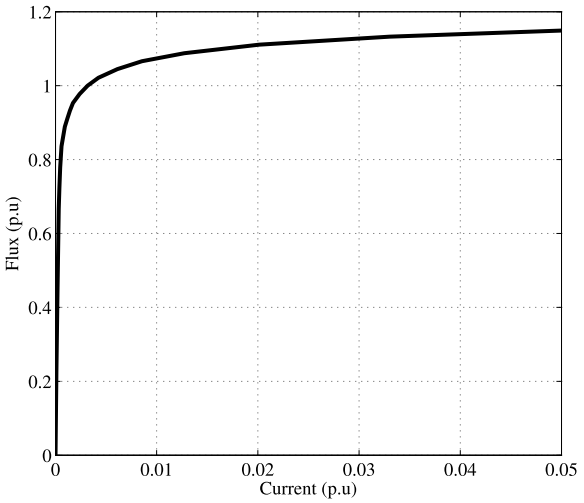

FIGURE 7. Typical *saturation curve* for distribution transformer core.

such sense the metal oxide surge arrester (MOSA) is evaluated in overvoltage conditions during ferroresonance.

The main characteristic of a surge arrester is that it provides a low-resistance path and limits overvoltages below the corresponding insulation level of equipment. In that sense, the surge arrester should act like an open circuit with an extremely high resistance during normal operation of the system and a relatively low resistance during overvoltages, limit transient voltages to a safe level, and bring the system back to its normal operational mode as soon as the transient voltages are suppressed; the surge arrester must have a non-linear voltage-current characteristic [28]. In this paper the arrester is represented in ATP/EMTP by using the surge arrester expression proposed by [29] and the expression is:

$$R(I) = R_0 \left[\frac{1 + A|I|^k}{1 + B(I)} \right] \tag{15}$$

where $R(I)$ is the non-linear resistance as a function of current in Ω, I is the current in amperes and the constants R_0, A, B and k are parameters for the non-linear resistance expression.

IV. FERRORESONANT CONDITION ASSESSMENT OF SWITCHING TRANSIENTS IN AN UNDERGROUND DISTRIBUTION SYSTEM

A. SYSTEM PARAMETERS

The electric power system portion used is represented in Figure 8 and simulated in ATP/EMTP [13]; this corresponds to an underground distribution feeder that is fed by a 23 kV bus through one 230/23 kV step-down three-phase transformer (T1) and a medium voltage cable system, that includes three coaxial XLPE cables and one bare conductor as Earth Continuity Conductor (ECC). On the load side, a distribution transformer of 500 kVA capacity (T2) where a load of 0.220 kV is connected.

The transmission system is represented by a 230 kV source with Thevenin equivalent of $Z_1 = 2.8282 + j\ 8.4412\ \Omega$ and $Z_0 = 0.60750 + j\ 6.5611\ \Omega$. and one power transformer of 60 MVA, 230/23 kV, Z = 12%, with Ynyn connection.

The transformer parameters are, 500 kVA 23Y:0.22Y kV, with dispersion impedance of $Z_p = 1.672 + j26.08\ \Omega$ and $Z_s = 0.0001549 + j.0024\ \Omega$. The Table 1 shows the saturation curve in *RMS* values utilized in the distribution transformer. The cable parameters of 25 kV 1x(Cu 1000kCM + Cu 250 kCM) and their physical and electrical characteristics utilized are shown in Table 2, and Table 3 shows the physical arrangement of conductors. The parameters of transformers and cables are obtained from manufacturers according to nameplate capacity, and then are processed to be used in ATP/EMTP software.

TABLE 1. Saturation curve of transformer wye-grounded/ wye-grounded connection.

Current (A)	Flux (Wb)
0.01689	14.853
0.05067	30.849
0.16892	49.510
0.50678	59.856
1.68928	64.579
5.06786	66.068
16.8928	66.606

TABLE 2. Physical and electrical characteristics of 23 kV cable.

Core	Inner	0.00000 m
	Outer	0.01335 m
	Resistivity	1.85300×10^{-8} $ohm \cdot m$
Insulation	Inner	2.80 cm
	Outer	5.50 cm
	Permittivity	2.70000
Metal Sheat	Inner	0.02295 m
	Outer	0.02359 m
	Resistivity	2.024×10^{-7} $ohm \cdot\ m$
Outer Cover	Inner	6.3500 cm
	Permittivity	5.0000

The distribution transformers are equipped with surge arresters to protect against over-voltages. In this sense, the model of metal-oxide surge arrester (MOSA) includes the following characteristics: $U_r = 21\ kV$, $U_c = 17\ kV$, $U_{res\ 30/60} = 61\ kV$, $U_{res\ 8/20} = 76\ kV$, $U_{res\ 1/20} = 84\ kV$

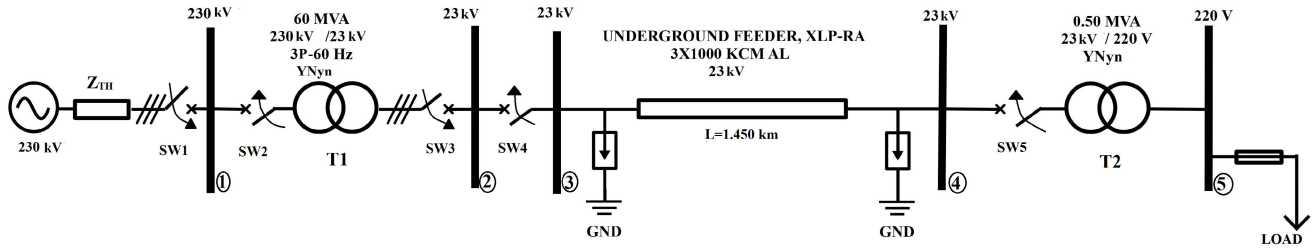

FIGURE 8. Underground distribution system used in the study.

TABLE 3. Conductor coordinates.

Phase	*x*-axis (m)	*y*-axis (m)
a	0.0280	-1.5485
b	-0.0280	-1.5485
c	0	-1.5000
ECC	0.0389	-1.5109

and $f = 60\ Hz$. The voltage-current relation of MOSA is shown in Table 4.

TABLE 4. Metal oxide surge arrester (MOSA) non-linear characteristics.

Current (A)	Voltage (V)
1500.0	65873.3
3000.0	68644.4
5000.0	71403.5
10000	76891.8
20000	84739.9

As a result of the evaluation in the ATP/EMTP LCC module considering the manufacturing characteristics from Table 2 and the physical coordinates in Table 3, the obtained parameters are shown in Table 5.

TABLE 5. The underground line parameters.

Data	R(Ω)	L(Ω)	C(μ F)
Positive Sequence	0.1684	0.319	0.5723
Zero Sequence	1.0633	0.8369	0.8687

V. RESULTS AND DISCUSSIONS

A. SIMULATION OF THE ENERGIZING THE FEEDER

Considering a typical vacuum circuit breaker operation, with a nominal voltage of 23 kV and rated current equal to 1250 A, it presents the switching sequence on times from registers; $ta = 07:30:07.409142$ s, $tb = 07:30:07.409373955$ s, and $tc = 07:30:07.410142$ s. It can be analyzed that the angular difference between ta and tb is $\theta_{ab} = 0.04989°$, between tb and tc is $\theta_{bc} = 0.16610°$and between tc and ta is $\theta_{ca} = 0.21599°$.

The Fig. 8 shows five switches, all of them are closed, except the $SW4$, which is closed in following the switching sequence described as follows:

Taking into account the typical times from the circuit breaker, the time inception in phase a is $t = 54.091$ ms, then the phase b is switching on in $t = 54.093$ ms. Remarkably, the switching time in phase c, $t = 54.101$ ms will not show ferroresonance due to the short time between switching on. In this case, it is supposed that the phase c was not appropriately operated (or the switching maneuvers are manual) and is energized 100 ms after the phase b was energized $t = 154.101$ ms. The obtained voltages in the primary side of transformer T2 (node 4 from Fig. 8) are shown in Fig. 9 where it can be observed that in $t = 54.093$ ms an induced overvoltage is observed in phase c with erratic waveform with possible sub-harmonics and quasi-periodic behavior that corresponds to ferroresonance characteristics, Finally, after that the phase c is closed in $t = 154.101$ ms, normal steady state is observed in the three phases.

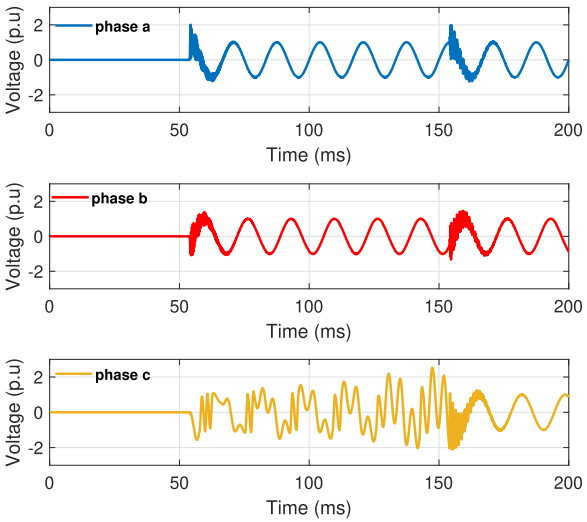

FIGURE 9. Voltage signal after switching on (close) the phases:(a) t = 54.091 ms, (b) t = 54.093 ms and (c) t = 154.101 ms.

Figure 10 shows the dissipated energy by the surge arrester when the $SW4$ is switching on the circuit. It can be observed

the dissipated energy by the surge arrester in phase c when the overvoltage appears.

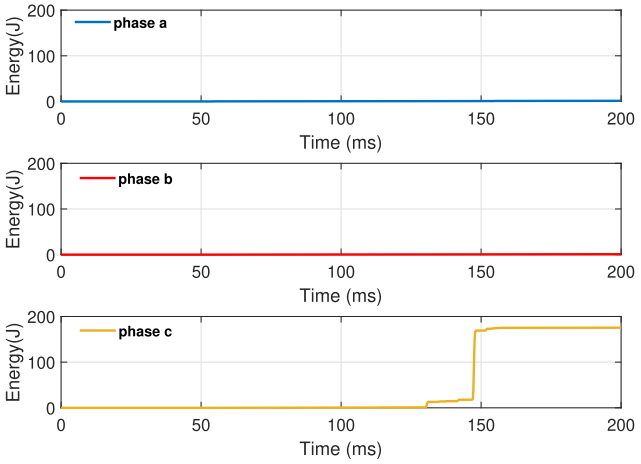

FIGURE 10. **Energy after switching on the phases.**

B. SIMULATION TO DE-ENERGIZING THE FEEDER

Taking into account the typical values of switching off times from vacuum circuit breaker of 23 kV, where the time register is shown as follows: the switching off time in phase a is $ta = 08 : 43 : 07.376913$ s, $tb = 08 : 43 : 07.373580$ s, and $tc = 08 : 43 : 07.376913$ s. where the angular difference between ta and tb is $\theta_{ab} = 0.719927°$, between tb and tc is $\theta_{bc} = 0.719927°$ and between tc and ta is $\theta_{ca} = 0.00000°$.

Furthermore, considering that the transformer $T2$ from Fig. 8 has been energized for a long time and then is switching off. Then, supposing that the phase a did not properly open (some manual maneuvers, etc.) and remains closed. Then, as is indicated in the breaker, phase b is open in $t = 53.735$ ms, and phase c is open in $t = 53.769$ ms. In this condition, with the phase a closed, the induced sustained overvoltage with possible sub-harmonics is observed in phases b and c as is shown in Fig. 11.

Finally, Fig. 12 shows the dissipated energy by using surge arresters during the switching off in phases b and c where the overvoltage is present. In both cases, open or close, if the time is not large enough, the surge arrester is not a risk; otherwise, they could be damaged.

C. FERRORESONANCE ANALYSIS UNDER DIFFERENT CONDITIONS

In this section, a summary of different scenarios was evaluated whit the aim to observe overvoltages (OV) under different maneuvers. The switching on and switching off can cause the ferroresonance phenomenon, mainly when the switching time between the poles is long enough. That condition is presented by using single-phase switching or the employment of fuses. On the other hand, when the circuit breakers are utilized, the phenomenon did not appear.

The Table 6 shows the simulations of the underground system of 23 kV with wye-grounded/wye-grounded (Ynyn)

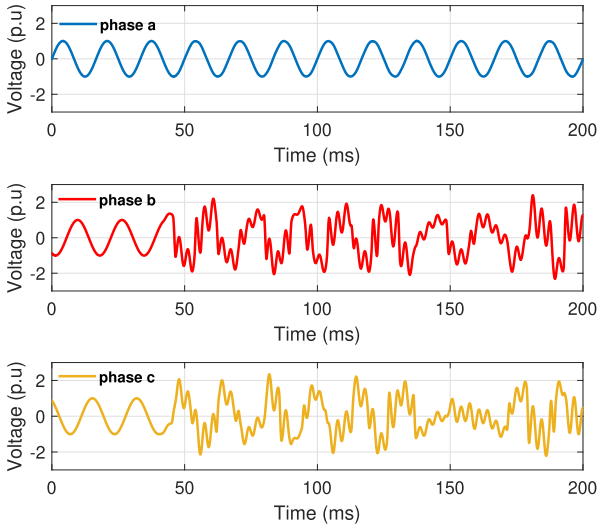

FIGURE 11. **Voltage signal after switching off (open) the phases: (a) t = closed, (b) t = 53.735 ms and (c) t = 53.769 ms.**

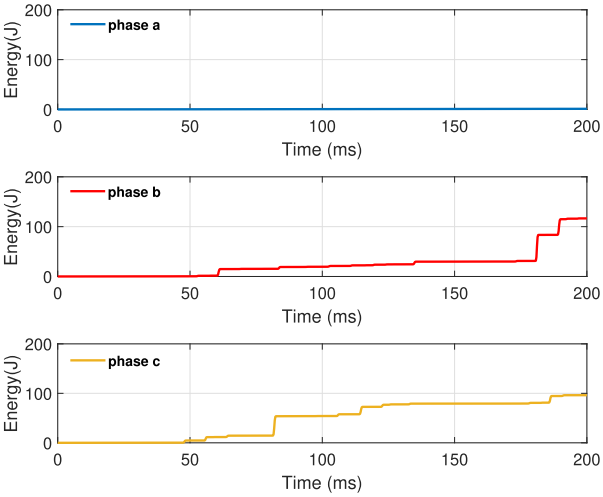

FIGURE 12. **Energy after switching off the phases.**

connection, and by using different switching times, following the order:

- Case 1.- Switching on the underground system.
- Case 2.- Switching off the underground system.
- Case 3.- Switching on the underground system with a surge arrester.
- Case 4.- Switching off the underground system with a surge arrester.
- Case 5.- Switching on with load at 20 percent of nominal.
- Case 6.- Switching off with load at 20 percent of nominal.

As shown in the summary of the simulation reported in Table 6, it can be observed that cases 1 and 2 where the non-simultaneous switching on and off leads to the ferroresonance with overvoltages up to 2.6731 p.u. and 2.6149 p.u., respectively. On the other hand, when surge

TABLE 6. Ferroresonance analysis with wye grounded-wye-grounded transformer connection.

Case	Switch	Time (ms)	Voltage (p.u)	OV
Case 1	Closed	ta=54.09142	1.0000	Yes
		tb=54.09373	1.0000	
		tc=154.09373	2.6731	
Case 2	Open	ta=200.0000	1.0000	Yes
		tb=53.7358	2.6149	
		tc=53.7691	2.4953	
Case 3	Closed	ta=54.0914	1.0000	Yes
		tb=54.0937	1.0000	
		tc=154.0937	2.5339	
Case 4	Open	ta=200.0000	1.0000	Yes
		tb=53.7358	2.6021	
		tc=53.7691	2.3696	
Case 5	Closed	ta=54.0914	1.0000	Yes
		tb=54.0937	1.0000	
		tc=154.0937	1.3725	
Case 6	Open	ta=200.0000	1.0000	No
		tb=53.7358	0.5006	
		tc=53.7691	0.4934	

arresters are employed, in cases 3 and 4, the ferroresonance phenomenon is damped with overvoltages up to 2.5339 p.u. and 2.6021 p.u., respectively. Finally, cases 5 and 6 show that the ferroresonance does not appear with a light load of up to 20% of the nominal load. However, overvoltage magnitudes were observed with slight load, for example, switching on with 10% of load yielded an overvoltage of 1.7122 p.u., an overvoltage of 1.8753 p.u. was reached with a 4% of load, and 2% of load produced an overvoltage magnitude equals to 1.9226 p.u. On the other hand, switching off with 2%, 4%, and 10% did not show any overvoltage.

VI. CONCLUSION

Circuit breakers commonly energize the feeders of a distribution substation with switching times very fast for closing or opening per phase differing from one another very little. Such disparity is associated with the physical speed of the mechanism of the circuit breaker depending on its type and model. In the worst cases, the operation with sectioning blades can reach in seconds, being the worst scenario of ferroresonance condition. The arrangement of underground cables with a transformer can facilitate the occurrence of ferroresonance. Still, if the switching is carried out from the circuit breaker of the substation there is no chance of ferroresonance. However, if a similar condition is presented in energizing distribution transformers in feeders with single poles or fuses, there is a high probability of occurrence.

As a result of the maneuvers evaluation of the main feeder with wye-grounded/wye-grounded transformer connection, the overvoltages related to the ferroresonance phenomenon were observed. For the discussed case 1, corresponding to the circuit energization, voltages around 2.631 p.u. were observed, while in case 2 (de-energizing the circuit) voltages of 2.6149 p.u. were reached. In both cases, the waveform presented an erratic behavior. In addition, In cases 3 and 4, the maneuvers of – *switching on and switching off*– were also addressed considering the transformer and surge arresters, whose results produced overvoltages of 2.5339 p.u. and 2.6021p.u. corresponding the cases 3 and 4, respectively. Besides, the energy dissipation in the surge arrester was observed. For cases 5 and 6, the transformer was loaded with 20% of their rated power during a maneuver of switching on and the results showed overvoltages around 1.3725 p.u (case 5); during the switching off (case 6), overvoltages were not observed. For a transformer loaded below 20% over its rated power, overvoltages were observed for switching-on cases with up to 2% of the load. On the contrary, switching-off cases did not show the ferrorresonance phenomenon when the load is below 20%. The ferroresonance phenomenon is dependent on the transformer design, connection type, cable system, load, transformer, etc. In fact, in real life, each system has its particular characteristics that should be modeled in deeper detail as much as possible. In such a sense, the simulations play an important role. For example, it has been observed that the surge arresters damped the overvoltage; nevertheless, is not the most common strategy to mitigate ferroresonance. As a result, if the overvoltage is sustained, the surge arresters, transformer, and electrical equipment can be damaged. It is important to mention that new underground distribution systems such as solar and wind power plants with different transformer connections may be susceptible to the ferroresonance phenomenon and should be analyzed.

REFERENCES

[1] *Resonance and Ferrorresonance in Power Networks*, document CIGRE Working Group C4.307, CIGRE, Technical Brochure 544, Feb. 2014.

[2] P. Boucherot, *Existence de Deux Rgimes en Ferrorsonance*. Rochester, NY, USA: R.G.E, Dec. 1920, pp. 827–828.

[3] H. Abdi, S. Abbasi, and M. Moradi, "Analyzing the stochastic behavior of ferroresonance initiation regarding initial conditions and system parameters," *Int. J. Electr. Power Energy Syst.*, vol. 83, pp. 134–139, Dec. 2016, doi: 10.1016/j.ijepes.2016.04.016.

[4] B. Behdani, M. Allahbakhshi, and M. Tajdinian, "On the impact of geomagnetically induced currents in driving series capacitor compensated power systems to ferroresonance," *Int. J. Electr. Power Energy Syst.*, vol. 125, Feb. 2021, Art. no. 106424, doi: 10.1016/j.ijepes.2020.106424.

[5] M. Mikhak-Beyranvand, J. Faiz, A. Rezaei-Zare, and B. Rezaeealam, "Electromagnetic and thermal behavior of a single-phase transformer during ferroresonance considering hysteresis model of core," *Int. J. Electr. Power Energy Syst.*, vol. 121, Oct. 2020, Art. no. 106078, doi: 10.1016/j.ijepes.2020.106078.

[6] M. Yang et al., "Electromagnetic transient study on flexible control processes of ferroresonance," *Int. J. Electr. Power Energy Syst.*, vol. 93, pp. 194–203, Dec. 2017, doi: 10.1016/j.ijepes.2017.05.026.

[7] H. R. A. Fordoei, H. Heydari, and S. A. Afsari, "Elimination of chaotic ferroresonance in power transformer by ISFCL," *Int. J. Electr. Power Energy Syst.*, vol. 68, pp. 132–141, Jun. 2015, doi: 10.1016/j.ijepes.2014.12.050.

[8] A. M. Abdel-Hamed, M. M. El-Shafhy, and E. A. Badran, "High ohmic reactor as a shunt limiter (HOR-SL) method for ferroresonance elimination in the distribution system," *IEEE Access*, vol. 10, pp. 134217–134229, 2022, doi: 10.1109/ACCESS.2022.3231190.

[9] U. Karaagac, J. Mahseredjian, and L. Cai, "Ferroresonance conditions in wind parks," *Electr. Power Syst. Res.*, vol. 138, p. 419, Sep. 2016, doi: 10.1016/j.epsr.2016.04.007.

[10] M. I. Mosaad and N. A. Sabiha, "Ferroresonance overvoltage mitigation using STATCOM for grid-connected wind energy conversion systems," *J. Modern Power Syst. Clean Energy*, vol. 10, no. 2, pp. 407–415, Mar. 2022, doi: 10.35833/MPCE.2020.000286.
[11] S. Rezaei, "An adaptive bidirectional protective relay algorithm for ferroresonance in renewable energy networks," *Electr. Power Syst. Res.*, vol. 212, Nov. 2022, Art. no. 108625, doi: 10.1016/j.epsr.2022.108625.
[12] G. S. Gokhale, B. A. Mork, J. O'Donnell, and S. R. Brehmer, "Ferroresonance case study in a distribution network and the potential impact of DERs and CVR/VVO," *Electr. Power Syst. Res.*, vol. 220, Jul. 2023, Art. no. 109303, doi: 10.1016/j.epsr.2023.109303.
[13] H. Kristian H. Idalen, L. Prikler, and F. Pealoza, *ATPDRAW Version 7.0 for Windows, Users' Manual*. Trondheim, Norway: Univ. Technology Trondheim, Norway, 2019.
[14] J.R. Marti, and A. Soundack, "Ferroresonance in power systems: Fundamental solutions," *IEE Proc. C Gener., Transmiss., Distrib.*, vol. 138, no. 4, pp. 321–329, 1991, doi: 10.1049/ip-c.1991.0040.
[15] G. Engdahl, "Ferroresonance in power systems," in *Grid Interference on Nuclear Power Plant Operations*, 2017, p. 457.
[16] H. Radmanesh and G. B. Gharehpetian, "Ferroresonance suppression in power transformers using chaos theory," *Int. J. Electr. Power Energy Syst.*, vol. 45, no. 1, pp. 1–9, Feb. 2013.
[17] A. E. A. Araujo, A. C. Soundack, and J. R. Marti, "Ferroresonance in power systems: Chaotic behaviour," *IEE Proc. C Gener., Transmiss., Distrib.*, vol. 140, no. 3, pp. 237–240, 1993, doi: 10.1049/ip-c.1993.0035.
[18] C. Kieny, G. L. Roy, and A. Sbai, "Ferroresonance study using Galerkin method with pseudo-arclength continuation method," *IEEE Trans. Power Del.*, vol. 6, no. 4, pp. 1841–1847, Oct. 1991, doi: 10.1109/61.97730.
[19] B. A. Mork and D. L. Stuehm, "Application of nonlinear dynamics and chaos to ferroresonance in distribution systems," *IEEE Trans. Power Del.*, vol. 9, no. 2, pp. 1009–1017, Apr. 1994, doi: 10.1109/61.296285.
[20] A. Djebli, F. Aboura, L. Roubache, and O. Touhami, "Impact of the eddy current in the lamination on ferroresonance stability at critical points," *Int. J. Electr. Power Energy Syst.*, vol. 106, pp. 311–319, Mar. 2019.
[21] M. Mikhak-Beyranvanda, J. Faizb, A. Rezaei-Zarec, and B. Rezaeealama, "Electromagnetic and thermal behavior of a single-phase transformer during Ferroresonance considering hysteresis model of core," *Elect. Power Energy Syst.*, vol. 121, Oct. 2020, Art. no. 106078.
[22] J. A. Corea, F. Gonzalez, and J. A. Martinez, "Tools for ferroresonance characterization," in *Proc. Eur. EMTP-ATP Users Group (EEUG) Conf.*, Zwickau, Germany, Sep. 2012, pp. 1–12.
[23] J. A. Martinez-Velasco, *Transient Analysis in Power Systems*. Hoboken, NJ, USA: Wiley, 2020.
[24] A. Ametani, T. Ohno, and N. Nagaoka, *Cable System Transients-Theory, Modelling and Simulation*. Singapore: Wiley, 2015, p. 6.
[25] *Cables for Medium Voltage Distribution*. Accessed: Aug. 2023. [Online]. Available: http://www.gomarbajio.com/fichas/CABLE/MEDIA-TENSION/COBRE-SELLADO/CONDUMEX.PDF
[26] *IEEE Guide for Application of Transformer Connections in Three-Phase Electrical Systems*, Standard C57.105-2019 (Revision of IEEE Std C57.105-1978), 2020, doi: 10.1109/IEEESTD.2020.9052773.
[27] E. Acha and M. Madrigal, *Power System Harmonics, Computer Modelling, and Analysis*. Hoboken, NJ, USA: Wiley, 2001, pp. 89–94.
[28] J. A. Martinez and F. Gonzalez-Molina, "Surge protection of underground distribution cables," *IEEE Trans. Power Del.*, vol. 15, no. 2, pp. 756–763, Apr. 2000, doi: 10.1109/61.853016.
[29] F. J. Peñaloza, "A practical arrester model for electromagnetic transient simulations," in *International Colloquium on Lightning and Power Systems*. Paris, France: CIGRE, 2018.

V. TORRES-GARCÍA (Senior Member, IEEE) received the M.Sc. and D.Sc. degrees in electrical engineering from Instituto Tecnológico de Morelia in 2009 and 2015, respectively. He is currently with PGIIE, TecNM Campus, Morelia. His current research interests include electric power systems, distribution networks, harmonics, electromagnetic transients, and power systems protections.

N. SOLÍS-RAMOS (Member, IEEE) received the M.Sc. degree in electrical engineering from the Autonomous National University of Mexico in 2017. He is currently with the Electricity Federal Commission, Mexico. His current research interests include distribution power systems, electromagnetic transients, and power systems protections.

N. GONZÁLEZ-CABRERA (Member, IEEE) received the degree in electrical engineering from the University of Guanajuato and the master's and D.Sc. degrees in electrical engineering from the Graduate and Research Program in Electrical Engineering (PGIIE), ITM. He is currently an Associate Professor with the Department of Electrical Energy, Universidad Nacional Autónoma de México. His current research interests include the operation and control of electrical power systems.

E. HERNÁNDEZ-MAYORAL (Member, IEEE) received the master's and D.Sc. degrees in electrical engineering from the Technological Institute of Morelia in 2010 and 2015, respectively. He was a Professor and a Researcher with Universidad del Istmo, Oaxaca, Mexico. He is currently a Cathedra-CONACyT with the Institute of Renewable Energies, Universidad Nacional Autónoma de México (UNAM). His current research interests include the analysis of energy quality in the interconnection of wind farms to the electric grid and smart electric microgrids.

DANIEL GUILLEN (Senior Member, IEEE) received the B.Eng. degree in electrical engineering from Instituto Tecnologico de Morelia, Mexico, in 2007, and the M.Sc. and Ph.D. degrees in electrical engineering from Universidad Autonoma de Nuevo Leon, Mexico, in 2010 and 2015, respectively. He was an Associate Professor with Universidad Nacional Autonoma de Mexico from 2016 to June 2018. He is currently with Tecnológico de Monterrey. His current research interests include power system modeling, power system protection, wide-area monitoring, signal processing, and transient analysis.